Thai Seismic Array (TSAR) Project

Satoru Tanaka[1)*], Weerachai Siripunvaraporn[2)3)], Songkhun Boonchaisuk[3)4)],

Sutthipong Noisagool[2)3)], Taewoon Kim[5)], Kenji Kawai[6)], Yuki Suzuki[6)],

Yasushi Ishihara[5)], Ryohei Iritani[7)], Koji Miyakawa[7)], Nozomu Takeuchi[7)]

and Hitoshi Kawakatsu[7)]

[1)] Volcanoes and Earth's Interior Research Center, Research Institute for Marine Geodynamics, Japan Agency for Marine-Earth Science and Technology

[2)] Department of Physics, Faculty of Science, Mahidol University

[3)] Thailand Center of Excellence in Physics, Commission on Higher Education

[4)] Geoscience Program, Mahidol University

[5)] Subduction Dynamics Research Center, Research Institute for Marine Geodynamics, Japan Agency for Marine-Earth Science and Technology

[6)] Department of Earth and Planetary Science, School of Science, The University of Tokyo

[7)] Earthquake Research Institute, The University of Tokyo

Abstract

Temporary broadband seismic observations, consisting of pilot and main observations, were conducted from January 2016 to January 2019 to study the seismic structure of the Earth's deep interior, and the crust and upper mantle structure beneath Thailand. Nearly fifty percent of the forty stations initially deployed were damaged by serious flooding and lightning. Nevertheless, the quality of the data collected permitted an analysis of local earthquakes and teleseismic signals. The data center at the Earthquake Research Institute, The University of Tokyo will provide continuous and event-edited seismograms, with state-of-health information (including clock information) from the spring of 2021.

Keywords： Thailand, broadband seismic observations

1. Introduction

Seismic properties at the core-mantle boundary (CMB) were previously interpreted based on the theory of the thermal boundary layer; however, several issues remained unresolved (Jones, 1977; Doornbos et al., 1986). Although the CMB is now considered to be a complex thermo-chemical boundary layer (Lay, 1989; Loper and Lay, 1995), with a phase transition of bridgemanite (Murakami et al., 2004; Lay et al., 2005), a general understanding of the CMB is far from a consensus. For instance, the heat flux at the CMB is currently estimated to be about 5-15 TW with large uncertainties, which requires a study of the temperature gradient at the base of the mantle (Lay et al., 2008). Global-scale seismic tomography has detected large low-shear-velocity provinces (LLSVPs) beneath Africa and the Pacific. Tomographic findings have been interpreted to represent segregated mid-ocean ridge basalt (MORB), a primitive high bulk modulus material of multiple components, and to have resulted from the fractional crystallization of a primordial dense basal magma ocean (Garnero et al., 2016).

To distinguish these scenarios, the resolutions of seismic images on regional and global scales need to be improved. To date, seismological studies have been conducted using several seismic arrays and nation-scale networks to detect several specific features. These studies discovered, for example, the presence of a low-velocity layer at the base of the mantle beneath the Tahiti hotspot (Tanaka, 2002), a ridge-like structure northwest of the Pacific LLSVP (Takeuchi, 2012), a sharp boundary at the western edge of the Pacific LLSVP (Takeuchi et al., 2008; Idehara et al., 2013), a rapid spatial variation along the western edge of the Pacific LLSVP (Tanaka et al., 2015), a regional scale S-wave velocity and anisotropic structures in the D″ region beneath the Hawaiian hotspot (Kawai and Geller, 2010a; Kawai and Geller, 2010b), and a highly localized low-velocity region at the base of the mantle beneath the Caroline hotspot (Konishi et al., 2014). These previous studies did not have the scope to address unresolved issues pertaining to the

lowermost mantle. New seismic observations were planned in Thailand, which is located where an active interaction between a subducted slab and the Pacific LLSVP is thought to occur and is, thus, an ideal site from which to study the lowermost mantle below the western Pacific.

Besides the lowermost mantle structure, the possible existence of a slightly low-velocity layer at the top of the core has been suggested (Tanaka, 2004; Tanaka, 2007), and has been the subject of many seismological studies (e.g., Alexandrakis and Eaton, 2010; Helffrich and Kaneshima, 2010; Kaneshima and Helffrich, 2013; Irving et al., 2018). Furthermore, Tanaka and Hamaguchi (1997) suggested that the uppermost 500 km of the inner core can roughly be divided into Asian (eastern) and American (western) hemispheres, referred to as a "hemispherical inner core." This has been researched through many observational studies (e.g., Creager, 1999; Niu and Wen, 2001; Waszek et al., 2011; Iritani et al., 2014), leading to investigations on the dynamics of the inner core and its relationship with the mantle and the outer core (e.g., Sumita and Olson, 1999; Alboussiere et al., 2010; Monnereau et al., 2010). However, seismologists need more data to study the outer and inner cores (Tkalčić, 2017).

The seismic observations in Thailand are also important to understand the geology of the Indochinese peninsula (Tapponnier et al., 1982) and seismic activity in this area. A moderately sized earthquake that occurred in northern Thailand in 2014 was found to have an interesting tectonic background (Noisagool et al., 2016). Noisagool et al. (2014) analyzed seismograms obtained from the Thai Meteorological Department to derive a map of the crustal thickness in Thailand using a teleseismic receiver function analysis and proposed a new tectonic structure that combines magnetic and gravity anomaly maps. However, the results appear to be preliminary due to sparse sampling in mainland Thailand.

The density of the seismic stations in Thailand is not as high as in neighboring regions (e.g., China and India). Thus, Japanese and Thai seismologists have been keen to establish seismic observations in Thailand. Broadband seismic observations with the Thai Seismic Array (TSAR) were initiated in January 2016, following deployment of two pilot stations in the "Seismic and geo-electromagnetic observation for core and mantle" project, which was funded by a KAKENHI Grant for Innovative

Areas. Array construction was completed in February 2017 with the installation of 40 stations. After project completion, the TSAR stations were dismantled in January 2019. The observed seismic data are stored at the data management center at the Ocean Hemisphere Research Center (Ocean Hemisphere Project Data Management Center; OHPDMC) within the Earthquake Research Institute (ERI), The University of Tokyo.

2. Observations
2.1 Basic information

The geographical distribution of TSAR stations, with the type of sensor deployed, is shown in Fig. 1. Station coordinates in WGS-84 were measured with etrex VISTA HCx (Garmin, Inc.) where uncertainty was less than 10 m. Station heights were estimated from Google Earth (Google, Inc.) because etrex height measurements were unstable and had low accuracy. The typical station interval is about 100 km, except in western Thailand. Fig. 2 shows the operating period of each station. One of the pilot stations, TS02, collected observations for nearly three years. Station information is listed in Table 1. Initially, 34 CMG-3T sets (Güralp, Inc.) and six sets of STS2 sensor (Streckeisen AG) with an RT130 data logger (Firmware version; 3.4.0, RETEK, Inc.) controlled by the iOS application iFSC (REFTEK, Inc.) were deployed. These sensors and data loggers
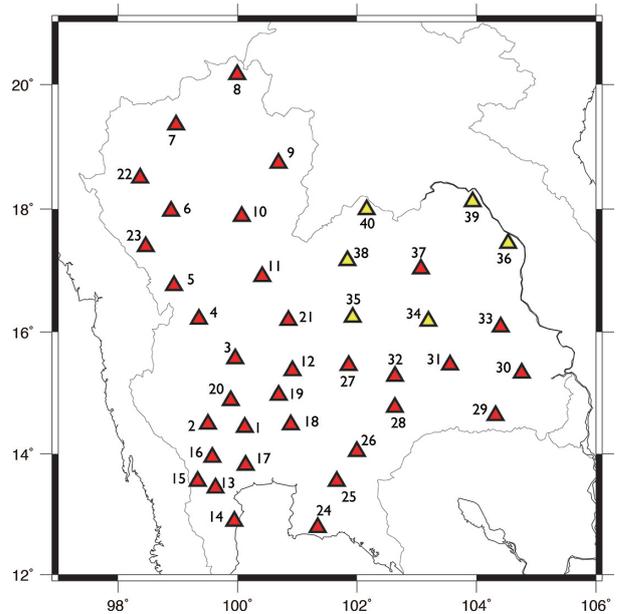

Fig. 1. Geographical distribution of seismic stations of the Thai Seismic Array (TSAR) as of February, 2017. Red and yellow triangles indicate CMG-3T and STS2, respectively.
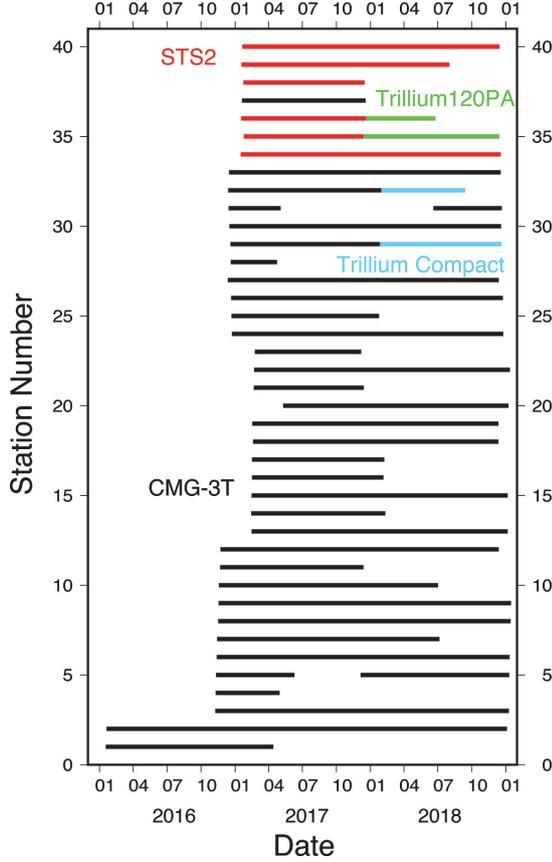
Fig. 2. Diagrams of the working period of the data loggers. Black, red, green, and blue lines represent working periods for combinations of CMG-3T and RT130, STS2 and RT130, Trillium120 PA and Taurus, and Trillium Compact All Terrain and Centaur, respectively.

belong to ERI and were previously used in the NECESSArray project (Tang et al., 2014). Given that the basement of the seismic stations was not hard, the RT130 data logger was configured so that the command for centering the pendulum mass position was automatically sent to the CMG-3T and STS2 every three and seven days, respectively. If the voltage corresponding to the mass position did not exceed 1.5 V, the CMG-3T would not respond, while the STS2 would always respond. Due to severe rain and flooding during the observation campaign, the sensors and data loggers at seven stations needed to be replaced. At three stations, i. e., TS05A, TS12A, and TS18A (shown in Table 1), the damaged CMG-3T sensors were replaced with those taken from the other stations where only the data acquisition systems were damaged and no further observations were being carried out. Two sets of Trillium 120 PA sensor (Nanometrics, Inc.) and Taurus data loggers (Firmware version; 3.7.6, Nanometrics, Inc.)

were used at stations TS35 and TS36, and two sets of Trillium compact All Terrain sensor (Nanometrics, Inc.) and Centaur data loggers (Firmware version; 3.2. 8, Nanometrics, Inc.) at stations TS29 and TS32. These stations are represented as TS29A, TS32A, TS35A, and TS36A in Table 1. The GPS clocks of RT130 were probably affected by lightning. According to log files, if the GPS clock was damaged, the time interval of the successful clock corrections would gradually increase and the GPS clock would fail. The damaged GPS clocks were replaced with those taken from the closed stations. Considering that the nominal accuracy of the crystal clock in RT130 is 10^{-7} when electric power is supplied, the clock shift is about 17 ms—which is less than the sampling interval of 25 ms—if the crystal clock runs freely without correction with a GPS signal for two days. With a clock accuracy of 0.1 s, it is acceptable for the clock to run for 12 days.

Three-component ground velocities with a sampling rate of 0.025 s (40 Hz) were acquired with 24-bit resolution by all data loggers. Additionally, voltage variations corresponding to mass positions, with a sampling interval of one minute, were recorded only with RT130. Thus, the volume of seismic data is about eight gigabytes (GB) for a half-year acquisition that is, on average, the typical operation period between data collection trips. If a station could not be visited for a long period of time, 32- or 64-GB compact flash drives (SanDisk Extreme, SanDisk Inc.) were used to store seismograms and associated data. Operation of these flash drives in severe environments, with temperatures ranging from −25 to 85 ℃, is guaranteed.

Fig. 3 schematically illustrates the station design. The sensor was set at the base of a 1 m depth hole, covered with a thermal insulator (glass wool) and a plastic bucket, and then buried in soil. The basement consisted of a concrete plate fixed with plaster. Electric power was supplied by a 70 W solar panel (Kyocela, Inc.), an 80 Ah sealed battery (made in Thailand), and a charge controller (Proster PM-15, Denryo, Inc.). To prevent an increase of temperature due to direct sunlight, the lower half of the box, including the data logger and batteries, was buried, then a thermal insulator was placed under the lid of the box. Finally, the box was covered with a plastic sheet and soil. The results of pilot observations indicated that the highest temperature of the data logger did not exceed 50℃ even in April, which is the hottest season in central Thailand. Photos 1(a)–(e) show

Table 1.   TSAR locations (WGS-84) and operating period.

Station Code	Latitude (°N)	Longitude (°E)	Height (m)	Operating Period yyyymmdd-yyyymmdd	Sensor
TS01	14.43871	100.12318	9	20160118-20170407	CMG-3T
TS02	14.49113	99.50581	126	20160120-20190104	CMG-3T
TS03	15.56395	99.96329	44	20161108-20190109	CMG-3T
TS04	16.21189	99.35447	147	20161109-20170506	CMG-3T
TS05	16.75896	98.93797	917	20161110-20170610	CMG-3T
TS05A	16.75896	98.93797	917	20171205-20190110	CMG-3T
TS06	17.96606	98.88839	435	20161112-20190111	CMG-3T
TS07	19.35491	98.97283	384	20161113-20180706	CMG-3T
TS08	20.16045	99.99616	435	20161116-20190114	CMG-3T
TS09	18.73975	100.68621	226	20161117-20190115	CMG-3T
TS10	17.88222	100.07197	232	20161118-20180702	CMG-3T
TS11	16.90598	100.41443	61	20161121-20171213	CMG-3T
TS12	15.36864	100.92047	99	20161122-20180201	CMG-3T
TS12A	15.36864	100.92047	99	20180201-20181213	CMG-3T
TS13	13.43600	99.63262	84	20170214-20190106	CMG-3T
TS14	12.88568	99.94721	9	20170213-20180210	CMG-3T
TS15	13.54815	99.33469	140	20170214-20190106	CMG-3T
TS16	13.94387	99.57963	40	20170215-20180205	CMG-3T
TS17	13.81242	100.13724	8	20170215-20180207	CMG-3T
TS18	14.48092	100.89311	15	20170218-20180202	CMG-3T
TS18A	14.48092	100.89311	15	20180202-20181212	CMG-3T
TS19	14.96616	100.68913	73	20170216-20181212	CMG-3T
TS20	14.87736	99.88810	36	20170510-20190108	CMG-3T
TS21	16.19340	100.85363	107	20170220-20171214	CMG-3T
TS22	18.50119	98.36971	498	20170221-20190112	CMG-3T
TS23	17.39216	98.46442	459	20170223-20171207	CMG-3T
TS24	12.78456	101.34288	29	20161223-20181225	CMG-3T
TS25	13.54792	101.66197	56	20161222-20180124	CMG-3T
TS26	14.04146	101.99926	73	20161221-20181224	CMG-3T
TS27	15.45523	101.86167	223	20161212-20181213	CMG-3T
TS28	14.76768	102.63510	207	20161220-20170424	CMG-3T
TS29	14.63114	104.32056	171	20161219-20180126	CMG-3T
TS29A	14.63114	104.32056	171	20180126-20181220	TrCmtAT[§]
TS30	15.32872	104.75815	135	20161216-20181219	CMG-3T
TS31	15.46296	103.55863	133	20161214-20181221	CMG-3T
				(20170504-20180619 stopped)	
TS32	15.27763	102.63778	159	20161213-20180130	CMG-3T
TS32A	15.27763	102.63778	159	20180130-20180913	TrCmtAT[§]
TS33	16.08472	104.40660	176	20161215-20181218	CMG-3T
TS34	16.17913	103.19643	162	20170116-20181218	STS2
TS35	16.24244	101.92924	241	20170124-20171214	STS2
TS35A	16.24244	101.92924	241	20171215-20181214	Tr120PA[†]
TS36	17.44519	104.53099	173	20170117-20171220	STS2
TS36A	17.44519	104.53099	173	20171220-20180625	Tr120PA[†]
TS37	17.02980	103.07098	182	20170119-20171219	CMG-3T
TS38	17.16560	101.84071	300	20170123-20171216	STS2
TS39	18.11949	103.93725	172	20170118-20180802	STS2
TS40	17.99013	102.16307	215	20170120-20181215	STS2

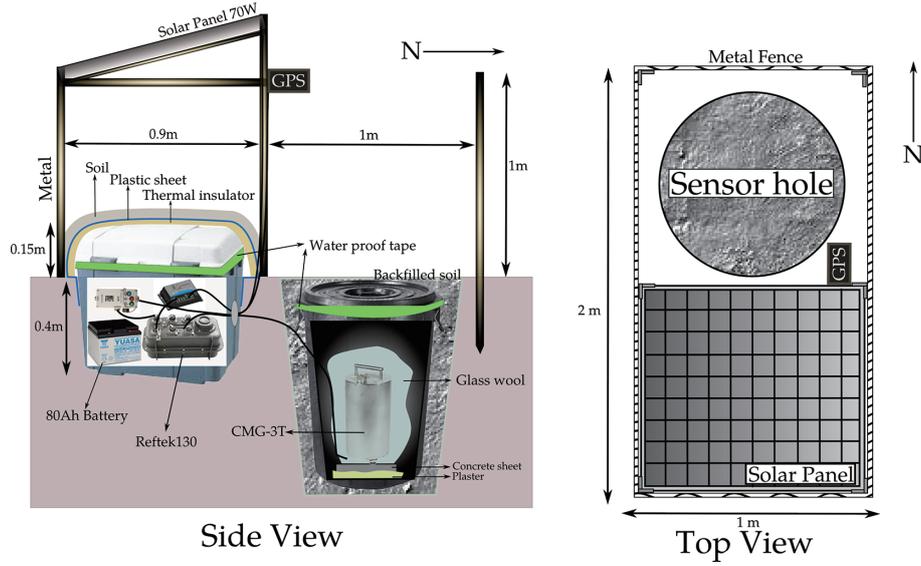[§] Trillium Compact All Terrain
[†] Trillium120PA

Fig. 3. Schematic image of the basic design of the seismic stations.

Photo 1. Snapshots of a series of a deployment process. (a) Digging a sensor hole. (b) Making up a basement. (c) Setting up a sensor with determination of the north-direction and leveling. (d) Putting a plastic bucket on the sensor and setting up the data logger, battery, etc., in the plastic box. (e) Fixing a solar panel and closing the logger box cover. (f) Completion of deployment. The station was enclosed with a wire-mesh fence.

typical deployment scenes. After construction, the station was enclosed with a wire-mesh fence as shown in Photo 1(f).

2. 2 Site survey, deployment, maintenance, and dismantling

From November 2015 to January 2016, site visits were made throughout Thailand to decide possible

station sites based on a noise survey with a Trillium Compact sensor (Nanometrics, Inc.) and a RT130 (REFTEK, Inc.). Negotiations were required with land owners. The tip of the Malay Peninsula, which is a politically sensitive area, was not included. Following advice from Thai members of the team, the team mainly visited schools that are typically more secure. Given that Thailand is susceptible to severe flooding during the rainy season, stations could not be installed near rivers or on floodplains. To confirm that the station design would work in the severe environment of Thailand, two pilot stations, TS01 and TS02, were constructed in close proximity to Bangkok. After the success of the pilot observations, one deployment team and one transportation team were organized. The deployment team, consisting of four persons with a car driver, loaded three to four sets of instruments into a pickup truck and left first. The transportation team consisting of one driver and one assistant loaded three to four sets of instruments into a box van and left Bangkok a few days afterwards. After deployment of the loaded instruments, the two teams met on the way to the deployment site and swapped the empty boxes and new instruments. The transportation team brought the empty boxes back to Mahidol University. Completing deployment of 38 stations, excluding the pilot stations, took four trips over a period extending from November 2016 to February 2017. The duration of each deployment trip was approximately two weeks, with a construction rate of one station per day. Given that digging a hole is the most time-consuming work, the Thai members of the team hired local labor and had the hole prepared prior to each deployment trip. It was originally planned to deploy the stations on the Malay Peninsula based on the results of the site survey. Unfortunately, due to heavy rain and severe flooding in January and February 2017, the deployment area had to be changed from the Malay Peninsula to the current area. As a result, a dense network was constructed in western Thailand.

The maintenance and data collection trips were conducted by Thai members of the team in the summers of 2017 and 2018, and by both Japanese and Thai team members in the winter of 2017. Sensors and data loggers at nearly half of the stations were damaged, probably due to severe flooding and the activities of wild animals and insects. In addition, lightning probably affected the GPS clocks.

Trips to dismantle the stations were conducted in December 2018 and January 2019. Similar to the deployment phase, dismantling was conducted by two teams: one team visited all the stations to dismantle the instruments, and the other team transported the empty boxes to the stations and brought the packed boxes back to Bangkok.

3. Results

3.1 Noise spectrum

Fig. 4 shows typical ground noise spectra of three components (Vertical: BHZ; North-South: BHN; East-West: BHE) at station TS13, which is one of the quiet sites. Although noise amplitudes at periods shorter than 1 s (frequencies higher than 1 Hz) differed largely from station to station, those at periods longer than 1 s (frequencies lower than 1 Hz) were almost the same as those shown in Fig. 4. If filters were not applied, ground noise at TS17 was very large because the station was located at the center of a populated area. However, ground noise at periods from 1 s to 20 s remained near the Low Noise
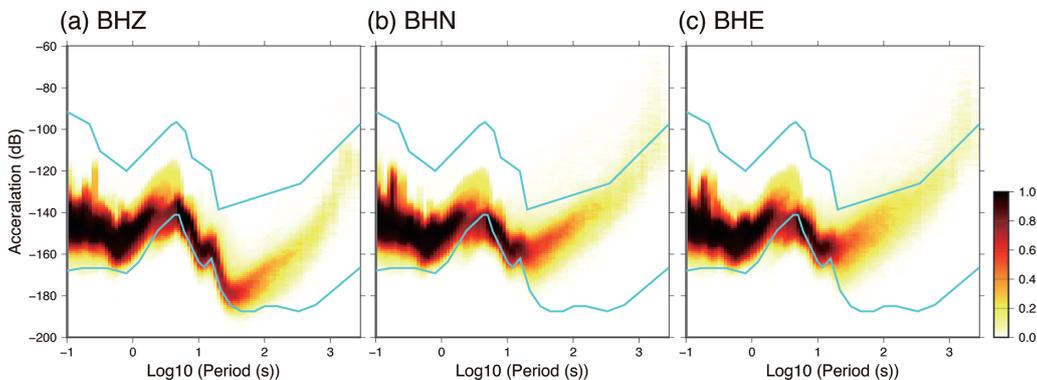

Fig. 4. Noise spectra of (a) UD (b) NS (c) EW components at TS13. Two blue lines denote new High Noise Model and new Low Noise Model (Peterson 1993).

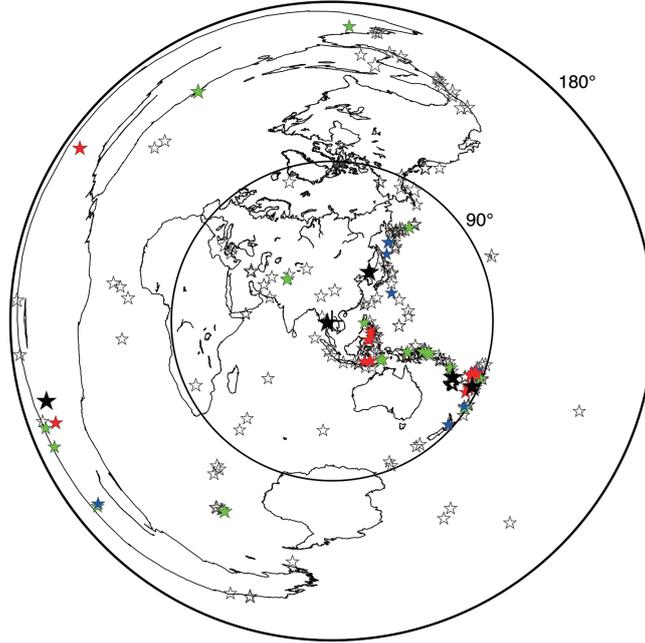## Epicenters from January 2017 to December 2018.

Fig. 5. Geographical distribution of epicenters with a magnitude greater than or equal to 6.0 from January 2017 to December 2018, on an azimuthal equidistant projection centered at (16° N, 102° E; the rough center of TSAR). White, green, blue, and red stars are epicenters with focal depths h of ($0 \leq h \leq 100$ km), ($100 < h \leq 200$ km), ($200 < h \leq 500$ km), and ($h \geq 500$ km), respectively. Black stars are epicenters mentioned in Figures 6–9.

Model (Peterson, 1993). Therefore, the noise levels of TSAR stations were quite low within this period range, which is essential for teleseismic body wave studies.

3. 2　Example seismograms

From January 2017 to December 2018, when more than half of the TSAR stations were operating, there were 245 earthquakes with magnitudes greater than or equal to 6.0, as shown in Fig. 5. These included the effects of a nuclear explosion on September 3, 2017 in North Korea. Fig. 6 shows the record of the vertical component, in which unknown phases as well as P and PcP phases can be identified. Deep earthquakes, which are mainly distributed in the southwestern Pacific and in South America, are expected to provide good-quality data that can be used to derive the structure of the mantle and the core. For instance, Figs. 7 a and 7b show horizontal component seismograms of earthquakes which occurred in Vanuatu and South Fiji, respectively. Figs. 7a and 7b are record sections of the north-south (NS) and east-west (EW) components, which are nearly tangential and radial components, respectively. In these record sections, ScS and SKS phases, which may include information on the structure above and below the CMB,

can be identified. Fig. 8 is a record of core phases from a Bolivian event, in which PKP-DF(PKIKP) and PKP-AB provided important information with which to elucidate the structures of the inner core and the CMB structure, respectively. A moderate earthquake (with a magnitude of ～ 5) occurred on December 30, 2018. The Thai Meteorological Department determined that the epicenter of the earthquake was located at 14.90° N, 99.14° E. Nine TSAR stations in western Thailand successfully recorded this event, as shown in Fig. 9. Thus, it is expected that TSAR data will contribute to hypocenter relocation and a further understanding of the source mechanism.

3. 3　Data archive

The format of the data retrieved from RT130 was originally defined by REFTEK. This format was converted into mini-SEED format using the software PASSCAL on a Macintosh operating system (e.g., rt130cut, ref2mseed, and rt2 ms from the PASSOFT package passcal-osx. 10.10. 2015. 169. pkg). The Nanometrics data loggers (Taurus and Centaur) directly acquired seismograms in mini-SEED format, as well as in the original data format defined by Nanometrics. Finally, the sensor and logger data were merged into the full-SEED format at the data

Nuclear explosion in North Korea
Origin time: 2017-09-03 03:30:01 M:6.0
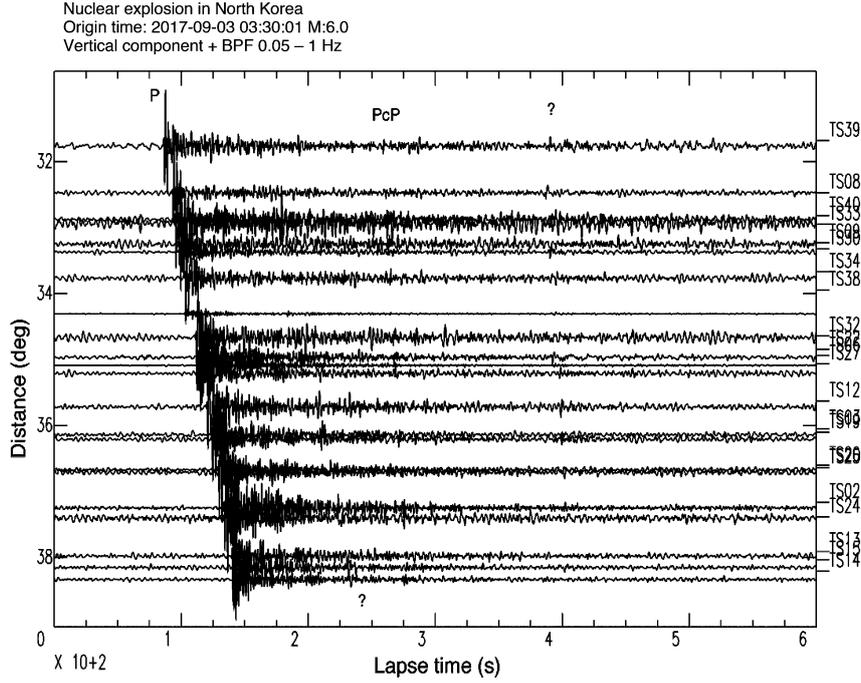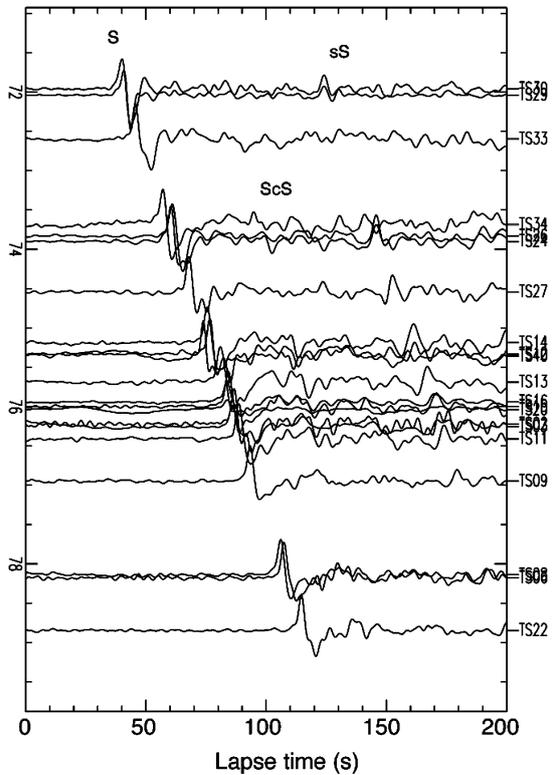Vertical component + BPF 0.05 – 1 Hz

Fig. 6.   Record section of vertical component for the nuclear explosion in North Korea on
September 3, 2017. Bandpass filter with 0.05–1.0 Hz is applied.

(a) Deep earthquake in Vanuatu
Origin Time: 2017-09-20 20:09:49 M:6.4
NS component + BPF 0.01 – 0.3 Hz

(b) Deep earthquake in South Fiji
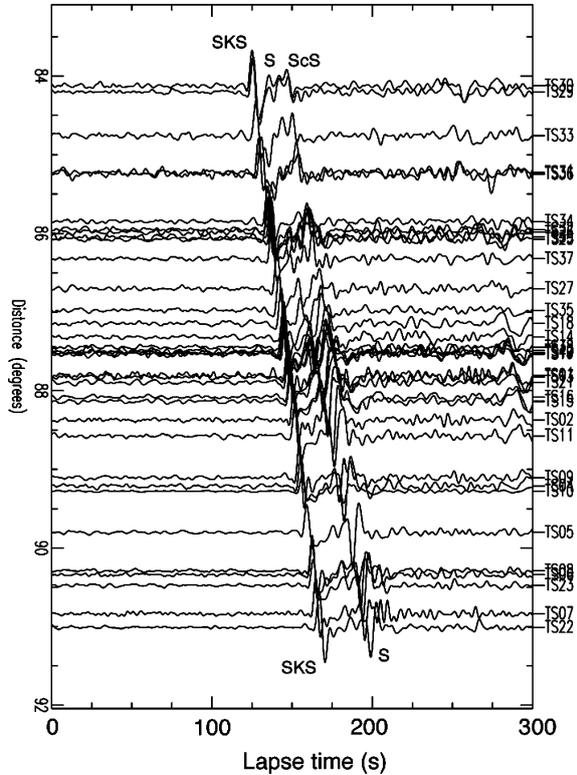Origin Time: 2017-02-24 17:28:45 M:6.9
EW component + BPF 0.01 – 0.3 Hz

Fig. 7.   Record sections of (a) NS component for the earthquake that occurred in Vanuatu, (b) of EW component for the
earthquake that occurred in south Fiji. Bandpass filter with 0.01–0.3 Hz is applied.

Fig. 8. Record section of vertical component for the earthquake that occurred in Bolivia. Bandpass filter with 0.02–1.0 Hz is applied.
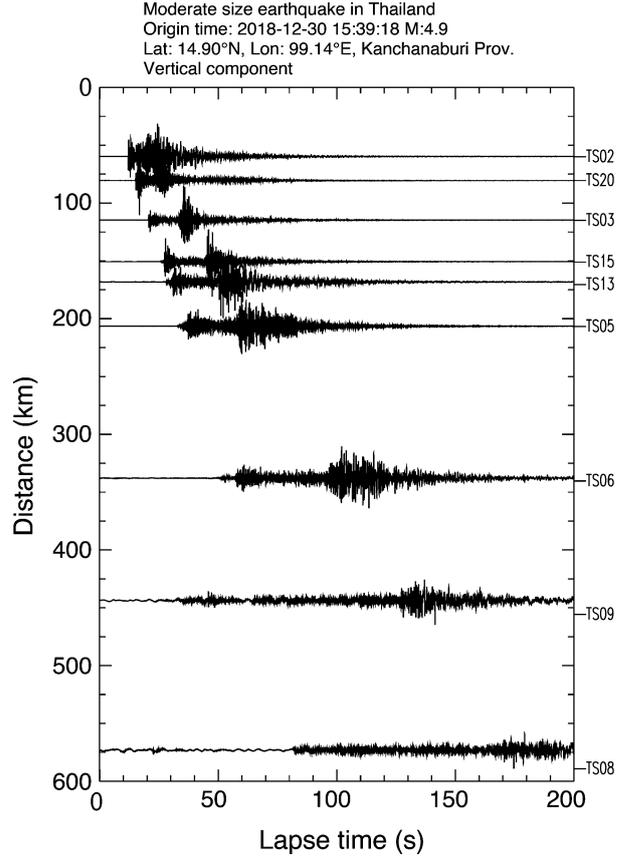

Fig. 9. Record section of vertical component for the earthquake that occurred in Kanchanaburi province, western Thailand. No bandpass filter is applied.

center. Although data availability is currently restricted to project members, all the data will be open two years after termination of the observation campaign, probably around the spring of 2021. The data center prepares web request pages for continuous observations (http://ohpdmc.eri.u-tokyo.ac.jp/breq-fast-tsar/index.html) and event data (http://ohpdmc. eri. u-tokyo. ac. jp/cgi-bin/dlevent-tsar/dlevent-tsar. pl), and provides full-SEED data through the Breq-Fast system.

Daily plots of the three components at live stations are available to the public at http://ohpdmc.eri.u-tokyo.ac.jp/wave/qdaily3.TSAR.html.

4. Discussion and ongoing analysis

One of the most important objectives of the TSAR project is to elucidate the finer structure of the lowermost mantle beneath the western Pacific because seismic waves from the deep earthquakes in the southwestern Pacific, especially the Tonga-Fiji region, can cast light on affected regions, as shown in Fig. 10.

Given that the epicentral distances between TSAR and Tonga-Fiji regions are greater than 85°, the SKS phases are separated well from S phases, as shown in Fig. 7b. This condition is suitable for analyzing shear wave splitting using SKS phases. In fact, SKS phases are observed both in the radial and transverse components, suggesting the existence of an anisotropic structure below Thailand. Many teleseimic P-waves can be observed at epicentral distances from 30 to 90° that are suitable for receiver function analyses; this is similar to the work of Noisagool et al. (2014). Such analyses will be helpful for revealing the fine crustal structure beneath Thailand.
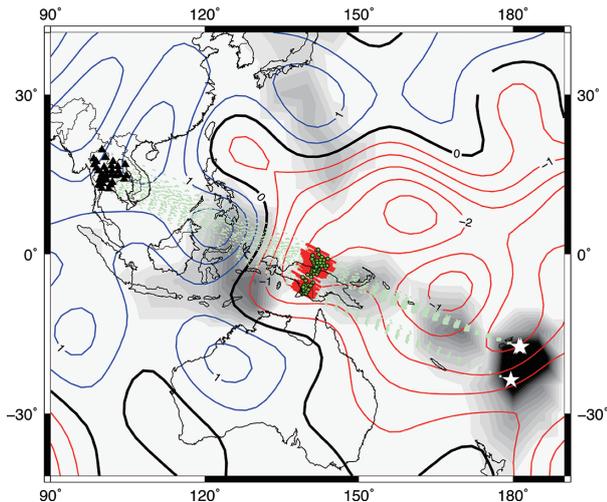
Fig. 10. Great circle paths (light green dashed lines) between hypocenters in Fiji regions (stars) to TSAR stations (triangles). Green dots represent the reflection points of ScS phases at the CMB. Red lines are the ray portions of ScS phases propagated in the lowermost 100 km of the mantle. Contour lines indicate S-wave velocity perturbation (Megnin and Romanowicz, 2000). Gray shaded areas are hypocentral regions for deep earthquakes in which dark gray corresponds to a high probability of occurrence.

References

Alboussiere, T., R. Deguen and M. Melzani, 2010, Melting-induced stratification above the Earth's inner core due to convective translation, *Nature*, **466**, 744–749.

Alexandrakis, C. and D.W. Eaton, 2010, Precise seismic-wave velocity atop Earth's core: No evidence for outer-core stratification, *Phys. Earth Planet. Inter.*, **180**, 59–65.

Creager, K. C., 1999, Large-scale variations in inner core anisotropy, *J. Geophys. Res.*, **104**, 23127–23139.

Doornbos, D.J., S. Spiliopoulos and F.D. Stacey, 1986, Seismological properties of D″ and the structure of a thermal boundary layer, *Phys. Earth Planet. Inter.*, **41**, 225–239.

Garnero, E.J., A.K. McNamara and S.H. Shim, 2016, Continent-sized anomalous zones with low seismic velocity at the base of Earth's mantle, *Nature Geoscience*, **9**, 481–489.

Goldstein, P. and A. Snoke, 2005, SAC Availability for the *IRIS* Community, https://ds.iris.edu/ds/newsletter/vol193/no1/193/sac-availability-for-the-iris-community/.

Goldstein, P., D. Dodge, M. Firpo and L. Minner, 2003, SAC2000: Signal processing and analysis tools for seismologists and engineers, in "*International Handbook of Earthquake and Engineering Seismology*", part B, edited by W.H.K. Lee, H. Kanamori, P.C. Jennings and C. Kisslinger, Academic Press, London, pp. 1613–1614.

Helffrich, G. and S. Kaneshima, 2010, Outer-core compositional stratification from observed core wave speed profiles, *Nature*, **468**, 807–810.

Idehara, K., S. Tanaka and N. Takeuchi, 2013, High-velocity anomaly adjacent to the western edge of the Pacific low-velocity province, *Geophys. J. Int.*, **192**, 1–6.

Iritani, R., N. Takeuchi and H. Kawakatsu, 2014, Intricate heterogeneous structures of the top 300 km of the Earth's inner core inferred from global array data: II. Frequency dependence of inner core attenuation and its implication, *Earth Planet. Sci. Lett.*, **405**, 231–243.

Irving, J.C.E., S. Cottaar and V. Lekic, 2018, Seismically determined elastic parameters for Earth's outer core, *Science Advances,* **4**, eaar2538.

Jones, G.M., 1977, Thermal interaction of core and mantle and long-term behavior of geomagnetic-field, *J. Geophys. Res.*, **82**, 1703–1709.

Kaneshima, S. and G. Helffrich, 2013, Vp structure of the outermost core derived from analysing large-scale array data of SmKS waves, *Geophys. J. Int.*, **193**, 1537–1555.

Kawai, K. and R.J. Geller, 2010a, Inversion of seismic waveforms for shear wave velocity structure in the lowermost mantle beneath the Hawaiian hotspot, *Phys. Earth Planet. Inter.*, **183**, 136–142.

Kawai, K. and R. J. Geller, 2010b, The vertical flow in the lowermost mantle beneath the Pacific from inversion of seismic waveforms for anisotropic structure, *Earth Planet. Sci. Lett.*, **297**, 190–198.

Konishi, K., K. Kawai, R.J. Geller and N. Fuji, 2014, Waveform inversion for localized three-dimensional seismic velocity structure in the lowermost mantle beneath the Western Pacific, *Geophys. J. Int.*, **199**, 1245–1267.

Lay, T., 1989, Structure of the core-mantle transition zone: A chemical and thermal boundary layer, *Eos Trans. Amer. Geophys. Union*, **70**, 49, 54–55, 58–59.

Lay, T., D. Heinz, M. Ishii, S.H. Shim, J. Tsuchiya, T. Tsuchiya, R.M. Wentzcovitch and D.A. Yuen, 2005, Multidisciplinary impact of the deep mantle phase transision in perovskite structure, *Eos Trans. Amer. Geophys. Union*, **86**, 1, 5.

Lay, T., J. Hernlund and B. Buffett, 2008, Core-mantle boundary heat flow, *Nature geoscience*, **1**, 25–32.

Loper, D.E. and T. Lay, 1995, The core-mantle boundary region, *J. Geophys. Res.*, **100**, 6397–6420.

Megnin, C. and B. Romanowicz, 2000, The three-dimensional shear velocity structure of the mantle from the inversion of body, surface and higher-mode waveforms, *Geophys. J. Int.*, **143**, 709–728.

Monnereau, M., M. Calvet, L. Margerin and A. Souriau, 2010, Lopsided Growth of Earth's Inner Core, *Science*, **328**, 1014–1017.

Murakami, M., K. Hirose, K. Kawamura, N. Sata and Y. Ohishi, 2004, Post-perovskite phase transition in $MgSiO_3$, *Science*, **304**, 855–858.

Niu, F. L. and L. X. Wen, 2001, Hemispherical variations in seismic velocity at the top of the Earth's inner core, *Nature*, **410**, 1081–1084.

Noisagool, S., S. Boonchaisuk, P. Pornsopin and W. Siripunvaraporn, 2014, Thailand's crustal properties from tele-seismic receiver function studies, *Tectonophysics*, **632**, 64–75.

Noisagool, S., S. Boonchaisuk, P. Pornsopin and W. Siripunvaraporn, 2016, The regional moment tensor of the 5 May 2014 Chiang Rai earthquake (Mw=6.5), Northern Thailand, with its aftershocks and its implication to the stress and the instability of the Phayao Fault Zone, *Journal of Asian Earth Sciences*, **127**, 231–245.

Peterson, J., 1993, Observations and modelling of seismic background noise, Open-file report 93–322, U.S. Geological Survey, doi:10.3133/ofr93322.

Sumita, I. and P. Olson, 1999, A laboratory model for convection in Earth's core driven by a thermally heterogeneous mantle, *Science*, **286**, 1547–1549.

Takeuchi, N., 2012, Detection of ridge-like structures in the Pacific Large Low-Shear-Velocity Province, *Earth Planet. Sci. Lett.*, **319–320**, 55–64.

Takeuchi, N., Y. Morita, N.D. Xuyen and N.Q. Zung, 2008, Extent of the low-velocity region in the lowermost mantle beneath the western Pacific detected by the Vietnamese Broadband Seismograph Array, *Geophys. Res. Lett.*, **35**, L05307.

Tanaka, S., 2002, Very low shear wave velocity at the base of the mantle under the South Pacific Superswell, *Earth Planet. Sci. Lett.*, **203**, 879–893.

Tanaka, S., 2004, Seismic detectability of anomalous structure at the top of the Earth's outer core with broadband array analysis of *SmKS* phases, *Phys. Earth Planet. Inter.*, **141**, 141–152.

Tanaka, S., 2007, Possibility of a low P-wave velocity layer in the outermost core from global SmKS waveforms, *Earth Planet. Sci. Lett.*, **259**, 486–499.

Tanaka, S. and H. Hamaguchi, 1997, Degree one heterogeneity and hemispherical variation of anisotropy in the inner core from PKP(BC)-PKP(DF) times, *J. Geophys. Res.*, **102**, 2925–2938.

Tanaka, S., H. Kawakatsu, M. Obayashi, Y.J. Chen, J.Y. Ning, S.P. Grand, F.L. Niu and J. Ni, 2015, Rapid lateral variation of P-wave velocity at the base of the mantle near the edge of the Large-Low Shear Velocity Province beneath the western Pacific, *Geophys. J. Int.*, **200**, 1050–1063.

Tang, Y., M. Obayashi, F. Niu, S. Grand, Y. J. Chen, H. Kawakatsu, S. Tanaka, J. Ning and J. Ni, 2014, Seismic evidence for a subduction-induced plume for the origin of Changbaishan volcanism in northeast China, *Nat. Geosci.*, **7**, 470–475.

Tapponnier, P., G. Peltzer, A. Y. Le Dain, R. Armijo and P. Cobbold, 1982, Propagating extrusion tectonics in Asia: New insights from simple experiments with plasticine, *Geology*, **10**, 611–616.

Tkalčić, H., 2017, *The Earth's inner core: Revealed by observational seismology*, Cambridge University Press, Cambridge, 223 pp.

Waszek, L., J. Irving and A. Deuss, 2011, Reconciling the hemispherical structure of Earth's inner core with its super-rotation, *Nat. Geosci.*, **4**, 264–267.

Wessel, P., W.H.F. Smith, R. Scharroo, J.F. Luis and F. Wobbe, 2013, Generic Mapping Tools: Improved version released, *Eos Trans. Amer. Geophys. Union*, **94**, 409–410.